Published in final edited form as:

Cancer Res. 2017 October 15; 77(20): 5687–5698. doi:10.1158/0008-5472.CAN-17-1353.

Phenotypic Heterogeneity of Circulating Tumor Cells Informs Clinical Decisions between AR Signaling Inhibitors and Taxanes in Metastatic Prostate Cancer

Howard I. Scher[1,6,*], **Ryon P. Graf**[2], **Nicole A. Schreiber**[1], **Brigit McLaughlin**[1], **Adam Jendrisak**[2], **Yipeng Wang**[2], **Jerry Lee**[2], **Stephanie Greene**[2], **Rachel Krupa**[2], **David Lu**[2], **Pascal Bamford**[2], **Jessica E. Louw**[2], **Lyndsey Dugan**[2], **Hebert A. Vargas**[3], **Martin Fleisher**[4], **Mark Landers**[2], **Glenn Heller**[5], and **Ryan Dittamore**[2]

[1]Genitourinary Oncology Service, Department of Medicine, Memorial Sloan Kettering Cancer Center, New York, New York

[2]Epic Sciences, La Jolla, California

[3]Department of Radiology, Memorial Sloan Kettering Cancer Center, New York, New York

[4]Clinical Chemistry Service, Department of Laboratory Medicine, Memorial Sloan Kettering Cancer Center, New York, New York

[5]Biostatistics Service, Department of Epidemiology and Biostatistics, Memorial Sloan Kettering Cancer Center, New York, New York

[6]Department of Medicine, Weill Cornell Medical College, New York, New York

Abstract

The heterogeneity of an individual patient's tumor has been linked to treatment resistance, but quantitative biomarkers to rapidly and reproducibly evaluate heterogeneity in a clinical setting are currently lacking. Using established tools available in a CAP-accredited and CLIA-certified clinical laboratory, we quantified digital pathology features on 9,225 individual circulating tumor cells (CTCs) from 179 unique metastatic castration-resistant prostate cancer (mCRPC) patients to define phenotypically distinct cell types. Heterogeneity was quantified based on the diversity of cell types in individual patient samples using the Shannon index and associated with overall survival (OS) in the 145 specimens collected prior to initiation of second or later lines of therapy. Low CTC phenotypic heterogeneity was associated with better OS in patients treated with androgen receptor signaling inhibitors (ARSI), whereas high heterogeneity was associated with better OS in patients treated with taxane chemotherapy. Overall, the results show that quantifying CTC phenotypic heterogeneity can help inform the choice between ARSI and taxanes in mCRPC patients.

[*]Address Correspondence to: Howard I. Scher, MD, Genitourinary Oncology Service, Department of Medicine, Sidney Kimmel Center for Prostate and Urologic Cancers, Memorial Sloan Kettering Cancer Center, 1275 York Avenue, New York, NY 10065, Phone: 646-422-4323 | Fax: 212-988-0851, scherh@mskcc.org.

Keywords

CTC; phenotypic heterogeneity; prostate cancer; biomarker

INTRODUCTION

The heterogeneity of cancer has long been recognized by phenotypic differences in cell morphology within a tumor specimen, and the observation that disease is rarely eliminated with any single systemic therapy. Recent multi-gene sequencing efforts have extended the concept of intra-patient cancer heterogeneity to the single cell (1,2), further revealing immense diversity in tumors between patients (3,4), individual lesions within the same patient (5,6), and different sites within each lesion (7,8). It is therefore unsurprising that reliance on solid tissue biopsies to guide “precision medicine” is not so precise (9,10). Recently reported profiling studies continue to elucidate the genomic complexity of cancer. Most are observational and are not reported as biomarkers that can be associated with clinical outcomes or used to impact medical decision making in patients (11,12). Here, we report the development of a quantitative biomarker of CTC heterogeneity fit-for-purpose (13) of informing treatment selection at the time a change in therapy is needed, and explore the relationship between CTC phenotypic heterogeneity and patient survival following treatment with androgen receptor signaling inhibitors (ARSI) or taxane chemotherapies.

It has been hypothesized that the efficacy of pathway-specific targeted agents would be inversely related to the degree of intra-patient heterogeneity present when a therapy is administered (8,14,15) (Supplemental Figure 1A–D). The currently approved standard of care life-prolonging systemic therapies for progressive metastatic castration-resistant prostate cancers (mCRPC) include two therapeutic drug classes: pathway-specific ARSI and non-pathway-specific taxane-based chemotherapy. ARSI, such as abiraterone acetate, enzalutamide and apalutamide, target the androgen receptor (AR) signaling pathway and inhibit the growth of cells dependent on AR signaling for survival, while taxane-based chemotherapies, docetaxel and cabazitaxel, stabilize microtubules, broadly inhibiting cell division in all cells, including those that harbor diverse drivers of resistance to targeted therapy (16).

In current clinical practice, the choice between one therapy over another at a decision point in mCRPC management is largely empiric; the biology of an individual patient’s cancer is typically not considered. In the 1st line setting following progression on androgen deprivation therapy (ADT), most patients are treated with an ARSI over a taxane based on the high response rates, more favorable safety profile, and long survival times at this decision point (17,18). This contrasts with the 2nd or later line setting where there is no consensus on management because the response to sequential ARSI is lower and of shorter duration, and response to the first does not predict response to the other (19). Every treatment to which a tumor has been exposed can alter the biology of the cancer (20), necessitating the serial profiling of disease. Validated therapy-guiding biomarkers to better inform each treatment decision is a significant unmet medical need (21).

High intra-tumor and intra-patient heterogeneity has been associated with poor prognosis in small patient cohorts of patients with breast and head and neck cancer (22,23) and more recently in lung cancer (24). Expanded explorations of the relationship between heterogeneity and other clinical outcomes have been hindered by the range of sampling methods to obtain tumor, the range of devices and analytical methods, and the lack of analytically and clinically validated assays. CTCs are a source of tumor material for biologic profiling that can be obtained from routine, repeated phlebotomy samples with minimal patient discomfort. CTCs can represent multiple metastatic lesions at once and are more likely to provide information on the diversity of a patient's disease than a single site biopsy. However, existing single-cell genomic techniques (25) have yet to meet the regulatory requirements of analytical and clinical validity, turn-around time and cost for more widespread clinical utility.

In contrast, automated phenotypic (protein and morphological) assessment of single cells has established clinical utility in the arena of cytological assessment of Pap smears for cervical cancer detection. In this report, we captured CTCs utilizing an analytically validated microscopy-based CTC detection technology (26) that allows for quantification of protein expression, and further characterized individual cells by digital pathology features previously validated and FDA approved for clinical use to identify and characterize malignant cells in Pap smears (27–29).

Our central hypothesis is that the degree of pre-therapy phenotypic heterogeneity of CTCs inversely associates with patient survival following treatment with ARSI but not taxane therapy. To test this, individual features in each cell were used to define phenotypically distinct cell types. Heterogeneity was then quantified based on the diversity of individual cell types in each patient sample using the Shannon index. The Shannon index is widely utilized in ecology and biodiversity research to measure the diversity or entropy of species, or in this case, CTCs. Previous applications of the Shannon index include showing differences in the genomic heterogeneity of separate and distinct metastatic lesions in an individual patient (30), and along with other measures, to predict the transition from Barrett's esophagus to esophageal adenocarcinoma (31). Here, we associated this quantitative heterogeneity biomarker with overall survival (OS) following treatment with standard of care drug classes to demonstrate clinical utility: that patient outcomes can be improved by using the heterogeneity biomarker test result to inform the choice of treatment relative to non-use of the test result. We also evaluated if observed phenotypic heterogeneity was associated with the presence of multiple genomic clones, elucidated by single-cell sequencing of CTCs in a subset of patient samples.

MATERIALS AND METHODS

Study Design

This is a retrospective analysis of a prospectively accrued cross-sectional cohort of patients treated in a clinical practice setting at Memorial Sloan Kettering Cancer Center (MSKCC). All patients provided signed informed consent for participation on a MSKCC Institutional Review Board/Privacy Board (IRB/PB) approved protocol prior to blood sampling and studies were conducted in accordance with the Declaration of Helsinki, Belmont Report and

U.S. Common Rule. The choice of therapy was at the discretion of the treating physician. All patients underwent a history that included details of the stage of disease at diagnosis, initial management, subsequent systemic therapies, physical examination, and laboratory studies including complete blood count, chemistry panel (albumin (ALB), alkaline phosphatase (ALK), lactate dehydrogenases (LDH), hemoglobin (Hgb), prostate specific antigen (PSA)), and serum testosterone to confirm castration status (<50 ng/dL) (Table 1).

Patient Selection

Between December 2012 and March 2015, 265 patients with histologically confirmed mCRPC undergoing a change in systemic therapy for progressive disease were treated at MSKCC. Of these, 179 unique patients starting an ARSI (abiraterone, enzalutamide or apalutamide) or taxane (docetaxel, cabazitaxel, or paclitaxel) provided 319 samples (221 pre-therapy and 98 on-therapy samples), which formed two cohorts of samples (Table 1, Figure 1). The first, the CTC contributing cohort, included all 319 samples and was used for automated feature extraction of protein biomarker expression and digital pathology features (Figure 2A). The second, the clinical association cohort, is a subset of the CTC contributing cohort that consists only of samples obtained prior to the start of the 2nd or later line therapy (86 ARSI and 59 taxane, or 145 total pre-therapy samples). First line samples were excluded because the majority of mCRPC patients progressing on standard hormones are treated with an ARSI due to the high response rate. Few receive taxanes in the 1st line, limiting the ability to explore the association of heterogeneity with outcome to both drug classes. There were no additional exclusions; all available samples were included in the analysis.

CTC Collection

Blood samples (7.5 mL) were collected in Streck tubes and processed at MSKCC or shipped to Epic Sciences and processed within 48 hours. Red blood cells were lysed, and approximately 3 million nucleated cells were dispensed onto 10–16 glass microscope slides and placed at −80 °C for long-term storage as previously described (26,32,33). Sample processing and testing were conducted in laboratories following both Clinical Laboratory Improvement Amendments (CLIA) and College of American Pathologists (CAP) regulations.

CTC Immunofluorescent Staining and Detection

CTCs were characterized by automated immunofluorescent staining for DAPI (a DNA stain), cytokeratins, CD45 (hematopoietic lineage marker), and AR N-terminal domain (AR) (Cell Signaling D6F11) as previously described (26,32,33). Up to two slides were evaluated per sample tested. CTCs were identified using fluorescent scanners that imaged every nucleated object on the slides. CTCs all had an intact nucleus (DAPI), no CD45 signal, and morphological features consistent with malignancy, as published previously (26). Clinical laboratory scientists (licensed in California) conducted final quality control of CTC identification.

Individual CTC Biomarker and Digital Pathology

We built upon digital pathology software from FDA-cleared devices used to characterize Pap smears for the context of use of diagnosing cervical cancer (27–29) to characterize CTCs. A systematic analysis performed by key leaders in the field identified the features that for decades were repeatedly found to be the most diagnostically meaningful in cytopathology, histopathology and hematopathology applications (34). A subset of these features was found to be suitable for the magnification of the microscope objectives utilized by the Epic Sciences platform. All features considered were measured, and part of the raw data used for analyses, listed in Figure 2A.

To allow for quantification of digital pathology features on a cell-by-cell basis, individual CTC images of cytokeratin (CK), nuclear, and AR N-terminal staining were segmented from each fluorescence channel image independently utilizing a library of single-cell features optimized for fluorescence microscopy (Figure 2A) (34). Features utilized for this analysis included morphometric and texture patterns of nuclear and CK staining, as well as the densitometric (intensity) of the CK and AR signal, which were quantified as a ratio of signal intensity on the CTC relative to surrounding white blood cells (WBCs) (Figure 2A). The identification of a cluster of two or more CTCs was recorded as a categorical dichotomous variable, as was whether the level of CK and AR expression was above or below an analytical threshold of intensity (Figure 2A) based on cultured cell line control cells spiked into healthy donor blood as previously described (26). Apoptotic CTCs were not included or reported, in part because nuclear fragmentation and membrane blebbing (35) confound the digital pathology features.

CTC Mathematical Phenotype Identification and Shannon index

Use of the Shannon index necessitated defining unique “species” within a given space. These “species” were defined using an unsupervised clustering analysis of the CTC protein, digital pathology, and categorical features (Figure 2B) into phenotypically similar subtypes of CTCs from all samples in the CTC contributing cohort. To enable cross-feature comparisons, minimize digital pathology feature redundancy, and distill the distinct sources of variance in the data, quantified biomarkers and features were z-score transformed prior to dimensionality reduction via principal component analysis, with the number of principal components selected via standard 85% variance inclusion (Supplemental Figure 2A).

K-means clustering was then used to group similar CTCs into discrete phenotypic cell subtypes based on the principal components of digital pathology features while minimizing the amount of variance of biomarker and feature ranges within each “cluster,” or group. The number of clusters (‘k’) was selected by the “elbow method” by which the within cluster sum of squares for k = 1 to k = 40 is plotted, and a human analyst looks for a bend in the curve, signifying a point of diminishing returns where partitioning the data into additional clusters (more ‘k’) only marginally adds to the similarity within each cluster (Supplemental Figure 2B). All CTCs in the cohort were then assigned a phenotypic cell subtype (‘A’-’O’) (Figure 3A–B) reflecting the mathematical unsupervised cluster (not to be confused with a histological cluster, or clump of CTCs traveling together within the bloodstream) and then grouped by their individual protein, digital pathology, and categorical features (Figure 4A).

Next, the patient-level frequency of the defined CTC phenotypic subtypes (categorized as 'A'-'O' / mL) were determined on a per sample basis (Figure 4B). These "species densities" were then utilized to calculate a Shannon index for each sample in the clinical association cohort (R package 'vegan') that quantified the entropy of the individual CTC phenotypic subtypes present at the time of the blood draw (Figure 4B). A higher Shannon index indicates both a higher number of different "species" (CTC phenotypic subtypes) present, as well as a more random distribution of those phenotypic subtypes, meaning that it would be more difficult, compared to lower Shannon index samples, to predict which phenotypic subtypes would be seen next given additional observation. If 0 or 1 CTCs were present, a value of zero is generated due to no sample present or the presence of only a single cell subtype.

Post-treatment Outcomes

Overall survival (OS) was calculated from initiation of therapy to death from any cause. Patients still alive at time of last follow-up were right-censored.

Statistical Analyses

Patient demographics and clinical characteristics at the time of blood draw were evaluated by descriptive statistics. Chi-squared and Wilcoxon rank sum tests were used to compare treatment groups for categorical and continuous characteristics, respectively. Median survival time as a function of a patient's continuous heterogeneity measure was evaluated using non-parametric kernel estimates (R package 'sm', (36)). Time-to-event outcomes, categorized by groups, were evaluated with the Kaplan-Meier method. Differences in time-to-event outcomes between categorized groups were evaluated using the maximum log-rank test, where the grouping was determined adaptively from the data (37).

The association of heterogeneity with time-to-event outcomes was additionally evaluated with hazard ratios estimated from univariable and multivariable Cox proportional hazards (PH) regression methods. Continuous variables with right-skewed distributions were transformed by $\log2(x + 1)$ to establish a normal distribution. The pre-therapy features evaluated for the multivariable Cox PH models included line of therapy (2, 3, or 4+, as factors), visceral metastases (present vs. not), pre-therapy PSA (continuous, log2 +1), LDH (continuous, log2 +1), ALK (continuous, log2 +1), Hgb (continuous), ALB (continuous), patient age (continuous), CTC/mL (continuous, log2 +1), Shannon index (continuous), and therapy class (taxane vs. ARSI). These pre-therapy features were individually assessed for correlation with Shannon index (Supplemental Figure 3).

Visceral metastases, patient age, and ALB were excluded from the final model by using a stepwise selection method based on univariate proportional hazards (Schoenfeld residuals $p > 0.05$) and univariate significance with outcome ($p < 0.05$). Included in the models is the interaction between Shannon index and therapy administered. CTC enumeration was also tested for an interaction with therapy and heterogeneity index because of its correlation to Shannon index. All earlier line samples from patients who contributed multiple pre-therapy samples but ultimately expired were right censored. Additionally, the robust sandwich estimate for the covariance matrix was implemented for all Cox PH models to correct for

possible underestimation of variance (38). All statistical tests were 2-sided and performed at the 5% significance level. Data consolidation was conducted using KNIME. Statistical analyses utilized the R packages: 'survival', 'stats', 'sm', 'vegan', and 'maxstat'. Graphical representations were generated with R packages: 'ggplot2', 'gridExtra', 'scales', 'survminer', and 'ggthemes'.

CTC Isolation, Genome Amplification, and Next-Generation Sequencing

Methods for CTC relocation, picking, and sequencing have been previously described (39,40). In brief, individual CTCs were relocated and recovered from assayed slides using the Eppendorf TransferMan NK4 micromanipulator. Single-cell whole genome amplification (WGA) was performed using the SeqPlex enhanced DNA amplification kit (Sigma). Shotgun libraries were constructed from 100ng of WGA material using the NEBNext Ultra DNA Library Prep Kit and sequenced to ~0.3X depth by 2x150 bp PE sequencing.

Genome wide copy number variation (CNV) analysis was performed using the Epic Sciences single-cell CNV analysis pipeline. FASTQ files were aligned to hg38 human reference genome from UCSC Genome database. BAM files were filtered for MAPQ 30 reads, followed by two separate analyses for genome-wide profiling (pipeline 1) and individual gene copy number changes determination (pipeline 2). Pipeline 1: Hg38 human genome was divided into ~3000 1M bp bins and counted across bins for each cell. Read counts per bin were normalized against WBC controls, and the circular binary segmentation algorithm (R Bioconductor package 'DNAcopy') was used to segment DNA copy number data (log2 normalized ratio, sample/reference) and identify abnormal copy number. Pipeline 2: Reads were counted for each gene and for each sample, and normalized against the total sequencing reads for the particular sample. Normalized reads were compared to reference WBCs and z-scores were calculated for each gene. Z-score of > 3 and < -3 are used as significant cutoff for calling gene gain or loss.

RESULTS

Clinical Characteristics of the Patient Population

A total of 179 unique patients contributed 319 samples prior to starting (221 pre-therapy) or while receiving (98 on-therapy) treatment with an ARSI or taxane therapy. Two cohorts of patient samples were studied: a CTC phenotypic analysis cohort (CTC contributing cohort), and a clinical association cohort that is a subset of the former (see Methods, Table 1 and Figure 1). The clinical association cohort included only the pre-therapy samples from patients about to start a 2nd or later line of systemic therapy for mCRPC.

Mathematical Phenotype Identification in Pre-therapy and On-therapy Samples

CTC phenotypic heterogeneity was evaluated using the Shannon index, which measures the entropy of species or, in this case, the phenotypically defined CTC subtypes (Figure 2B) Unsupervised clustering of all of the single-cell features (Figure 4A) from the 9225 CTCs identified from the 319 samples in the CTC contributing cohort revealed a k of 15 (Supplemental Figure 2B), which was used to "define" or classify individual cells into 15 phenotypic subtypes ('A'-'O') where the cells were more similar to members of the subtype

to which they were categorized relative to the other 14 subtypes (Figure 3). Each phenotypic subtype represents a unique signature of the single-cell features (Figure 4A). Each patient sample was then evaluated for the diversity of the defined CTC subtypes present in a blood draw, and quantified using the Shannon index (see Methods, Figure 4B). Examples of CTCs from low Shannon index (Figure 4C) and high Shannon index (Figure 4D) samples are shown.

Inter-Sample Shannon Index is Related to Overall Survival of ARSI, but not Taxanes

The relationship between Shannon index (phenotypic entropy) and OS following treatment with a pathway-specific targeted ARSI therapy or taxane chemotherapy was analyzed on a continuous basis with estimates of median survival by Shannon index (see Methods) separated by therapy administered (ARSI or taxanes) (Figure 5A). While median survival estimates remained constant for patients on taxanes with respect to Shannon index, the median survival of patients on ARSI was longer than taxane patients with comparable Shannon index at the low end. In contrast, patients with high Shannon index on ARSI had shorter median survival than those on taxanes with comparable Shannon index on the high end. This relationship was further visualized with Kaplan-Meier plots for each therapy class with patient populations dichotomized by the crossover point (Figure 5A, arrow). Patients going onto ARSI (Figure 5B) had a large difference in survival between “high” and “low” Shannon index samples (median OS: 8.8 months vs. 28.1 months, $p = 0.0015$), whereas patients going onto taxanes (Figure 5C) did not (11.4 months vs. 12.9 months, $p = 1$).

Multivariate Analyses

To correct for potential imbalances in the demographics of the pre-ARSI and pre-taxane patient samples due to greater use of the former in the 2nd line and the latter in the 3rd or later line setting, we evaluated survival in the context of a multivariate Cox PH model utilizing known prognostic factors (see Methods). Integrated into the Cox PH model was the interaction between CTC phenotypic entropy (Shannon index) and therapy class (taxanes vs. ARSI). CTC enumeration was also considered as an interaction term with therapy class (see Methods), and while there was an interaction (data not shown), the interaction between Shannon index and therapy class was stronger. Of note, there remained a significant interaction between increasing Shannon index and higher risk of death on ARSI relative to taxanes (HR: 2.48, 95% CI: 1.22 – 5.03, $p = 0.0119$) (Figure 5D–E), even when adjusting for pre-therapy prognostic factors. To assess the possibility that the observed treatment interaction effects are being driven by low Shannon index due to inclusion of samples with 0 or 1 CTCs, we created a separate model in which we excluded these samples and kept those from the clinical association cohort with a Shannon index greater than 0. The same trends as previously described were upheld (Supplemental Figure 4A–B).

The Pleomorphism Index

The relationship between phenotypic heterogeneity, drug class, and OS was additionally evaluated with an alternate measure of intra-patient phenotypic variance: the Pleomorphism index (see Supplemental Methods). Similar to the Shannon index, patients with low Pleomorphism index had longer survival on ARSI, and patients with high Pleomorphism

index had longer survival on taxanes, observed as a continuous marker in univariate and multivariate settings (Supplemental Figure 5A–B and Supplemental Figure 6A–E).

Heterogeneous Genomic Profiles Identify Frequent Subclonal Drivers of ARSI Resistance Observed in High Phenotypic Heterogeneity Samples

Randomly selected CTCs from 17 patient samples, each with 10 or more CTCs, were single-cell sequenced to assess intra-sample genomic heterogeneity with copy number variations (CNVs). From a time and resource perspective, it is currently impractical to individually sequence all CTCs in each sample to inform clinical decisions. However, we still sought to explore genomic heterogeneity at the single-cell level in a subset of samples using these research tools.

Shown are two examples of patient samples with multiple distinct genomic profiles with unique CNV patterns (Figure 6A–B). One patient (Figure 6A) had 22 CTCs sequenced and appears to have two major genomic patterns (I and II). Three sub-patterns were observed in pattern II with additional chromosome Y loss or a chr5q deletion, indicated by the red circles in Figure 6A. The second patient (Figure 6B) had 62 CTCs sequenced and four major genomic patterns identified (I-IV). Pattern II had many chromosomal breakpoints and alterations, including chr8p loss and 8q gain which commonly occur in prostate cancer, and III and IV had single chromosome loss or gain. This patient also had nine additional CTCs that did not fit any of the four major genomic patterns identified in Figure 6B, each instead representing its own unique pattern. These samples also had high Shannon index scores of phenotypic heterogeneity, and are provided as examples of the diverse genomic profiles observed in patient samples. They are not intended to offer correlations between phenotypic and genotypic heterogeneity. Properly powered comparisons between phenotypic and genotypic heterogeneity are planned for future work.

A limitation of this analysis is the reliance on CNVs, as the single-cell sequencing technique utilized does not measure mutations or translocations that could reveal additional inter-cellular diversity. For example, common driver mutations in prostate cancer include alterations like SPOP mutations, AR mutations, and ERG rearrangements which would not be seen with these CNV analyses but very well could exist in the flat genomes shown in Pattern I of Figure 6A and 6B.

A broader view of CTCs sequenced from high phenotypic heterogeneity samples showed varying degrees of subclonal gain or loss of key alterations known to drive resistance to ARSI (Figure 6C). No patients were dominated by what is a more-or-less clonal genotype (i.e. white or black, but not gray tiles). Instead, most patients had many “gray” areas representing subclonal alterations of other drivers, suggesting that a single dominant clone was not identified or not present across all CTCs.

Certain alterations appeared to be more clonal than others, such as MYC, which when amplified appeared in high proportions of CTCs within a patient sample. Other alterations, such as AR amplification, appeared frequently as subclones. These observations are consistent with intra-patient tumor clonality analyses (41), where MYC and AR amplifications identified in tissue biopsies to be primarily truncal and subclonal,

respectively, in a cohort of 10 autopsies. In contrast, the analyses reported here were conducted on cells from living patients, with the potential to use results to inform clinical decision making.

DISCUSSION

Developing biomarkers of heterogeneity to guide treatment selection and improve patient outcomes is an unmet medical need. Our objective was to develop a quantitative CTC heterogeneity biomarker assay that has achieved the level of method validation to be fit-for-purpose (13) of exploring its relationship to survival in mCRPC patients treated with an ARSI or taxane therapy. To do so, we retrospectively applied the Shannon index to prospectively collected and clinically annotated patient samples about to start a 2nd or later line of treatment. The analysis showed that patient survival on taxanes was unrelated to the degree of heterogeneity, while lower heterogeneity scores were associated with a longer median survival on ARSI relative to taxanes, and higher heterogeneity with shorter median survival on ARSI relative to taxanes. A significant interaction was also observed between the Shannon index (Figure 5D–E) and therapy class in multivariate models correcting for potential intra-cohort imbalances. The results support the hypothesis that CTC phenotypic heterogeneity measured prior to starting systemic therapy associates with differential outcomes on pathway-specific hormonal agents but not on non-pathway-specific chemotherapy.

As noted by a recent heterogeneity focus group, there are no standard methods to quantify heterogeneity, or consensus on whether the method to evaluate heterogeneity should be genetic, transcriptomic, phenotypic, epigenetic, or a combination thereof (42). All may prove relevant. It is critical to develop and test the association of a reproducibly measurable heterogeneity biomarker(s) with clinical outcomes: the context of use for which the biomarker result will be used to inform treatment decisions in the clinic. The outcome explored here was OS.

In this analysis we expanded upon previously validated digital pathology features that were components of FDA-cleared devices for single-cell characterization with proven clinical utility for detecting cervical cancers from cytology Pap smears and applied these same tools to characterize CTCs phenotypically. Relative to single-site biopsies, CTCs can originate from multiple tumor sites within a patient, and provide a more global picture of an individual patient’s cancer. In contrast to single-site biopsies, the acquisition of CTCs through phlebotomy poses minimal risk to the patient, and is amenable to repeated sampling to monitor disease evolution over time.

Critical to the assessment of intra-patient heterogeneity in CTCs is a CTC detection method that does not rely on pre-enrichment by epitope, size, or shape. These positive selection methods often miss critical CTC subtypes and do not consistently assess cell features essential to the analysis of heterogeneity. The CAP-accredited and CLIA-certified Epic Sciences platform used here has undergone the necessary analytical validation (accuracy, linearity, specificity, and intra/inter-assay precision) for CTC detection and enumeration (26) and has been previously demonstrated to detect a wide range of CTC phenotypes

(32,33,40,43). These include rare CTCs that are negative for epithelial markers with malignant genomics (40,43) and CTCs that are smaller than WBCs (32,43).

The approach used to analyze the digital pathology features represents a novel confluence of techniques adapted from diverse fields. The z-score transformation and principal component analysis is used in gene array applications to avoid redundancy and distill distinct sources of variance within the data (44). K-means clustering (45) is a machine learning technique with applications including, but not limited to, e-commerce, defense, ecology, and astronomy (46). Shannon index is a measure of species diversity frequently utilized in ecology research (47), where quantification and monitoring of species biodiversity and evolutionary events is common. Shannon index increases with both the number of unique species present and the evenness in species distribution. When applied to CTCs, it indicates the level of uncertainty to predict what phenotypic subtypes of CTCs are going to be detected next: the higher the uncertainty (entropy), the higher the heterogeneity. We additionally developed a simpler, alternate measure of CTC phenotypic heterogeneity within patient samples that does not require unsupervised clustering, the Pleomorphism Index (see Supplemental Methods, Supplemental Figure 5A–B), performed identical survival analyses, and observed similar results with respect to phenotypic heterogeneity, drug class administered, and OS (Supplemental Figure 6A–E). These results suggest that there are likely multiple ways to model heterogeneity, but the underlying phenomena observed is consistent with our central hypothesis.

A limitation of this approach is the potential lack of utility in the setting of low or no CTC counts. Recognizing this, as stated in the Methods, our focus was the 2nd or later line of therapy setting where the frequency of detection and individual CTC counts are higher, and the decision to select one form of therapy vs. another is more critical. In our analyses, samples with 1 or 0 CTCs were assigned a heterogeneity score of 0 and included in our OS association analyses. However, despite these potential shortcomings, Shannon index does demonstrate the ability to differentially predict OS by therapy class, even when total CTC count is included as a covariate in multivariate models. A supplemental sub-cohort analysis which excluded samples with heterogeneity scores of 0 yielded similar results as well (Supplemental Figure 4A–B). Ultimately, it may be concluded that the determination of a heterogeneity score (for which there is currently no unified definition, units or reference range determined by the field (42) might have a requisite minimal number of CTCs for optimal quantification.

Another emerging technique that can infer heterogeneity on the genomic level is cell-free DNA (cfDNA) (48). cfDNA is several steps removed from the cells of origin and represents a homogenized mixture, or pool, of tumor DNA and non-tumor DNA from multiple cells, which poses additional technical hurdles when trying to distill features of entropy or variance within a patient sample. cfDNA can also include fragments of apoptotic or dead cells which could represent parts of tumor that were sensitive to the treatment and consequently eliminated (49). In part due to these reasons, we excluded analysis of apoptotic CTCs and only scored intact, whole CTCs.

In addition to clinical utility, the abilities to provide results in time to inform clinical decisions and at a reasonable cost are essential for the use of a biomarker in clinical practice. Image-based phenotypic measures of tumor heterogeneity meet this requirement. Previously, our group analytically validated a single-CTC whole genome sequencing technology (39) to potentially assess intra-patient genomic heterogeneity. While promising, this approach is not scalable with available sequencing technologies when considering reproducibility, turnaround time and cost. Acknowledging these caveats, we performed whole genome sequencing on CTCs from a subset of samples with at least 10 evaluable CTCs. The results showed frequent subclonal alterations associated with ARSI resistance (Figure 6C), consistent with the poor outcome of patients on ARSI who had high phenotypic heterogeneity determined with the Shannon index reported herein (Figure 5). A greatly expanded cohort of single-cell sequencing results would be required for meaningful statistical analyses of genomic heterogeneity. However, these data suggest that samples with high phenotypic heterogeneity have heterogeneous genomic profiles as well.

In previous work, we studied an analytically validated immunohistochemical assay for AR-V7 as a treatment-selection biomarker for the same context (50), and found that 100% of patients with nuclear-localized AR-V7 protein in their CTCs had poor responses on ARSI and lived longer on taxanes (50). The assay, however, did not identify all patients who would have poor response on ARSI, as the frequency of AR-V7 detection was only 20% among patients who had less than 50% PSA decline by 12 weeks. Thus, most of the patients who did not respond to ARSI were AR-V7-negative. In the current study, patients with an increasing Shannon index had an increasing risk of death on ARSI *relative to* taxanes (Figure 5). This suggests that patients with low heterogeneity scores would be more likely to survive longer on an ARSI over a taxane, and patients with high heterogeneity scores would likely survive longer on a taxane than an ARSI. Specifically in the context of AR-V7-negative patients, this measure could have the potential to more reliably inform treatment selection at this clinical decision point. Comparisons of AR-V7 to heterogeneity indices are planned for future studies.

CTC heterogeneity biomarkers may also be useful in the clinical development of novel therapies, as many trials evaluate cohorts of heavily pre-treated patients who might exhibit high levels of heterogeneity that could portend resistance to targeted therapeutics. Such patients may be more suitably offered participation in studies of novel drug combinations, or combinations that include a cytotoxic drug more likely to affect diverse cell populations.

While the results reported here have the potential for broad implications, this study was designed to test a hypothesis that represents a first step in the clinical evaluation of an analytically valid, quantitative measurement of heterogeneity that could serve as a therapy-guiding biomarker to inform the choice between an ARSI or taxane for mCRPC patients starting a 2nd or later line of therapy. The gold standard for evaluating the clinical utility of a predictive biomarker is through randomized, interventional trials. A limitation of observational studies like this one is the possibility of unobserved confounding factors. An additional limitation of our study is the lack of an external validation cohort. Definitive clinical utility of these heterogeneity biomarkers will require a sequence of trials, analogous to the development of a drug focused on a context of use. Further clinical validation in

separate, larger cohorts is planned and assessment of longitudinal and kinetic changes over time in response to therapy are ongoing, both within the context of mCRPC clinical decisions and outside of prostate cancer.

Supplementary Material

Refer to Web version on PubMed Central for supplementary material.

Acknowledgments

Financial Support: Equal distributions of funds from NIH/NCI P50-CA92629 SPORE in Prostate Cancer, NIH/NCI Cancer Center Support Grant P30-CA008748, Department of Defense Prostate Cancer Research Program (PC121111 and PC131984), Prostate Cancer Foundation Challenge Award, and David H. Koch Fund for Prostate Cancer Research were used to support the design and conduct of the study.

We would like to thank the patients and their families for taking part in this study, and the clinical and laboratory staff at MSKCC and Epic Sciences.

References

1. Pestrin M, Salvianti F, Galardi F, De Luca F, Turner N, Malorni L, et al. Heterogeneity of PIK3CA mutational status at the single cell level in circulating tumor cells from metastatic breast cancer patients. Molecular oncology. 2015; 9(4):749–57. DOI: 10.1016/j.molonc.2014.12.001 [PubMed: 25539732]
2. Paguirigan AL, Smith J, Meshinchi S, Carroll M, Maley C, Radich JP. Single-cell genotyping demonstrates complex clonal diversity in acute myeloid leukemia. Science translational medicine. 2015; 7(281):281re2.doi: 10.1126/scitranslmed.aaa0763
3. Roberts NJ, Norris AL, Petersen GM, Bondy ML, Brand R, Gallinger S, et al. Whole Genome Sequencing Defines the Genetic Heterogeneity of Familial Pancreatic Cancer. Cancer discovery. 2016; 6(2):166–75. DOI: 10.1158/2159-8290.cd-15-0402 [PubMed: 26658419]
4. Skoulidis F, Byers LA, Diao L, Papadimitrakopoulou VA, Tong P, Izzo J, et al. Co-occurring genomic alterations define major subsets of KRAS-mutant lung adenocarcinoma with distinct biology, immune profiles, and therapeutic vulnerabilities. Cancer discovery. 2015; 5(8):860–77. DOI: 10.1158/2159-8290.cd-14-1236 [PubMed: 26069186]
5. Brastianos PK, Carter SL, Santagata S, Cahill DP, Taylor-Weiner A, Jones RT, et al. Genomic Characterization of Brain Metastases Reveals Branched Evolution and Potential Therapeutic Targets. Cancer discovery. 2015; 5(11):1164–77. DOI: 10.1158/2159-8290.cd-15-0369 [PubMed: 26410082]
6. Russo M, Siravegna G, Blaszkowsky LS, Corti G, Crisafulli G, Ahronian LG, et al. Tumor Heterogeneity and Lesion-Specific Response to Targeted Therapy in Colorectal Cancer. Cancer discovery. 2016; 6(2):147–53. DOI: 10.1158/2159-8290.cd-15-1283 [PubMed: 26644315]
7. Gerlinger M, Rowan AJ, Horswell S, Larkin J, Endesfelder D, Gronroos E, et al. Intratumor heterogeneity and branched evolution revealed by multiregion sequencing. The New England journal of medicine. 2012; 366(10):883–92. DOI: 10.1056/NEJMoa1113205 [PubMed: 22397650]
8. Burrell RA, McGranahan N, Bartek J, Swanton C. The causes and consequences of genetic heterogeneity in cancer evolution. Nature. 2013; 501(7467):338–45. DOI: 10.1038/nature12625 [PubMed: 24048066]
9. Hiley C, de Bruin EC, McGranahan N, Swanton C. Deciphering intratumor heterogeneity and temporal acquisition of driver events to refine precision medicine. Genome biology. 2014; 15(8): 453.doi: 10.1186/s13059-014-0453-8 [PubMed: 25222836]
10. McGranahan N, Favero F, de Bruin EC, Birkbak NJ, Szallasi Z, Swanton C. Clonal status of actionable driver events and the timing of mutational processes in cancer evolution. Science translational medicine. 2015; 7(283):283ra54.doi: 10.1126/scitranslmed.aaa1408

11. Alberter B, Klein CA, Polzer B. Single-cell analysis of CTCs with diagnostic precision: opportunities and challenges for personalized medicine. Expert review of molecular diagnostics. 2016; 16(1):25–38. DOI: 10.1586/14737159.2016.1121099 [PubMed: 26567956]
12. Gorges TM, Kuske A, Rock K, Mauermann O, Muller V, Peine S, et al. Accession of Tumor Heterogeneity by Multiplex Transcriptome Profiling of Single Circulating Tumor Cells. Clinical chemistry. 2016; 62(11):1504–15. DOI: 10.1373/clinchem.2016.260299 [PubMed: 27630154]
13. Cummings J, Raynaud F, Jones L, Sugar R, Dive C. Fit-for-purpose biomarker method validation for application in clinical trials of anticancer drugs. British journal of cancer. 2010; 103(9):1313–7. DOI: 10.1038/sj.bjc.6605910 [PubMed: 20924371]
14. Swanton C. Intratumor heterogeneity: evolution through space and time. Cancer research. 2012; 72(19):4875–82. DOI: 10.1158/0008-5472.can-12-2217 [PubMed: 23002210]
15. Crockford A, Jamal-Hanjani M, Hicks J, Swanton C. Implications of intratumour heterogeneity for treatment stratification. The Journal of pathology. 2014; 232(2):264–73. DOI: 10.1002/path.4270 [PubMed: 24115146]
16. NCCN Clinical Practice Guidelines in Oncology: Prostate Cancer. 2016.
17. Ryan CJ, Smith MR, de Bono JS, Molina A, Logothetis CJ, de Souza P, et al. Abiraterone in metastatic prostate cancer without previous chemotherapy. The New England journal of medicine. 2013; 368(2):138–48. DOI: 10.1056/NEJMoa1209096 [PubMed: 23228172]
18. Beer TM, Armstrong AJ, Rathkopf DE, Loriot Y, Sternberg CN, Higano CS, et al. Enzalutamide in metastatic prostate cancer before chemotherapy. The New England journal of medicine. 2014; 371(5):424–33. DOI: 10.1056/NEJMoa1405095 [PubMed: 24881730]
19. Schrader AJ, Boegemann M, Ohlmann CH, Schnoeller TJ, Krabbe LM, Hajili T, et al. Enzalutamide in castration-resistant prostate cancer patients progressing after docetaxel and abiraterone. European urology. 2014; 65(1):30–6. DOI: 10.1016/j.eururo.2013.06.042 [PubMed: 23849416]
20. Gillessen S, Omlin A, Attard G, de Bono JS, Efstathiou E, Fizazi K, et al. Management of patients with advanced prostate cancer: recommendations of the St Gallen Advanced Prostate Cancer Consensus Conference (APCCC) 2015. Annals of oncology : official journal of the European Society for Medical Oncology / ESMO. 2015; 26(8):1589–604. DOI: 10.1093/annonc/mdv257
21. Scher HI, Morris MJ, Stadler WM, Higano C, Basch E, Fizazi K, et al. Trial Design and Objectives for Castration-Resistant Prostate Cancer: Updated Recommendations From the Prostate Cancer Clinical Trials Working Group 3. Journal of clinical oncology : official journal of the American Society of Clinical Oncology. 2016; 34(12):1402–18. DOI: 10.1200/jco.2015.64.2702 [PubMed: 26903579]
22. Seol H, Lee HJ, Choi Y, Lee HE, Kim YJ, Kim JH, et al. Intratumoral heterogeneity of HER2 gene amplification in breast cancer: its clinicopathological significance. Modern pathology : an official journal of the United States and Canadian Academy of Pathology, Inc. 2012; 25(7):938–48. DOI: 10.1038/modpathol.2012.36
23. Mroz EA, Tward AD, Pickering CR, Myers JN, Ferris RL, Rocco JW. High intratumor genetic heterogeneity is related to worse outcome in patients with head and neck squamous cell carcinoma. Cancer. 2013; 119(16):3034–42. DOI: 10.1002/cncr.28150 [PubMed: 23696076]
24. Jamal-Hanjani M, Wilson GA, McGranahan N, Birkbak NJ, Watkins TBK, Veeriah S, et al. Tracking the Evolution of Non–Small-Cell Lung Cancer. New England Journal of Medicine. 2017; null. doi: 10.1056/NEJMoa1616288
25. Navin NE. The first five years of single-cell cancer genomics and beyond. Genome research. 2015; 25(10):1499–507. DOI: 10.1101/gr.191098.115 [PubMed: 26430160]
26. Werner SL, Graf RP, Landers ML, Valenta DT, Schroeder M, Greene SB, et al. Analytical Validation and Capabilities of the Epic CTC Platform: Enrichment-Free Circulating Tumour Cell Detection and Characterization. Journal of Circulating Biomarkers. 2015; 4(3)
27. Wied GL, Bahr GF, Oldfield DG, Bartels PH. Computer-assisted identification of cells from uterine adenocarcinoma. A clinical feasibility study with TICAS. I. Measurements at wavelength 530 nm. Acta cytologica. 1968; 12(5):357–70. [PubMed: 5245328]

28. Zahniser DJ, Oud PS, Raaijmakers MC, Vooys GP, Van de Walle RT. BioPEPR: a system for the automatic prescreening of cervical smears. The journal of histochemistry and cytochemistry : official journal of the Histochemistry Society. 1979; 27(1):635–41. [PubMed: 86581]
29. Tucker JH, Shippey G. Basic performance tests on the CERVIFIP linear array prescreener. Analytical and quantitative cytology. 1983; 5(2):129–37. [PubMed: 6881762]
30. Almendro V, Kim HJ, Cheng YK, Gonen M, Itzkovitz S, Argani P, et al. Genetic and phenotypic diversity in breast tumor metastases. Cancer research. 2014; 74(5):1338–48. DOI: 10.1158/0008-5472.can-13-2357-t [PubMed: 24448237]
31. Maley CC, Galipeau PC, Finley JC, Wongsurawat VJ, Li X, Sanchez CA, et al. Genetic clonal diversity predicts progression to esophageal adenocarcinoma. Nature genetics. 2006; 38(4):468–73. DOI: 10.1038/ng1768 [PubMed: 16565718]
32. Beltran H, Jendrisak A, Landers M, Mosquera JM, Kossai M, Louw J, et al. The Initial Detection and Partial Characterization of Circulating Tumor Cells in Neuroendocrine Prostate Cancer. Clinical cancer research : an official journal of the American Association for Cancer Research. 2015; doi: 10.1158/1078-0432.ccr-15-0137
33. Punnoose EA, Ferraldeschi R, Szafer-Glusman E, Tucker EK, Mohan S, Flohr P, et al. PTEN loss in circulating tumour cells correlates with PTEN loss in fresh tumour tissue from castration-resistant prostate cancer patients. British journal of cancer. 2015; doi: 10.1038/bjc.2015.332
34. Rodenacker K, Bengtsson E. A feature set for cytometry on digitized microscopic images. Analytical cellular pathology : the journal of the European Society for Analytical Cellular Pathology. 2003; 25(1):1–36. [PubMed: 12590175]
35. Wickman G, Julian L, Olson MF. How apoptotic cells aid in the removal of their own cold dead bodies. Cell death and differentiation. 2012; 19(5):735–42. DOI: 10.1038/cdd.2012.25 [PubMed: 22421963]
36. Scher HI, Jia X, de Bono JS, Fleisher M, Pienta KJ, Raghavan D, et al. Circulating tumour cells as prognostic markers in progressive, castration-resistant prostate cancer: a reanalysis of IMMC38 trial data. The Lancet Oncology. 2009; 10(3):233–9. DOI: 10.1016/s1470-2045(08)70340-1 [PubMed: 19213602]
37. MIller R, Siegmund D. Maximally Selected Chi Square Statistics. Biometrics. 1982; 38(4):1011–6.
38. Lin DY, Wei LJ. The Robust Inference for the Proportional Hazards Model. Journal of the American Statistical Association. 1989; 84:1074–8.
39. Greene SB, Dago AE, Leitz LJ, Wang Y, Lee J, Werner SL, et al. Chromosomal Instability Estimation Based on Next Generation Sequencing and Single Cell Genome Wide Copy Number Variation Analysis. PLOS ONE. 2016; 11(11):e0165089.doi: 10.1371/journal.pone.0165089 [PubMed: 27851748]
40. Anantharaman A, Friedlander TW, Lu D, Krupa R, Premasekharan G, Hough J, et al. Programmed death-ligand 1 (PD-L1) characterization of circulating tumor cells (CTCs) and white blood cells (WBCs) in muscle invasive and metastatic bladder cancer patients. Journal of clinical oncology : official journal of the American Society of Clinical Oncology. 2016; 34(suppl 2S) abstr 446.
41. Gundem G, Van Loo P, Kremeyer B, Alexandrov LB, Tubio JM, Papaemmanuil E, et al. The evolutionary history of lethal metastatic prostate cancer. Nature. 2015; 520(7547):353–7. DOI: 10.1038/nature14347 [PubMed: 25830880]
42. Alizadeh AA, Aranda V, Bardelli A, Blanpain C, Bock C, Borowski C, et al. Toward understanding and exploiting tumor heterogeneity. Nature medicine. 2015; 21(8):846–53. DOI: 10.1038/nm.3915
43. McDaniel AS, Ferraldeschi R, Krupa R, Landers M, Graf R, Louw J, et al. Phenotypic diversity of circulating tumour cells in patients with metastatic castration-resistant prostate cancer. BJU international. 2016; doi: 10.1111/bju.13631
44. Cheadle C, Vawter MP, Freed WJ, Becker KG. Analysis of microarray data using Z score transformation. The Journal of molecular diagnostics : JMD. 2003; 5(2):73–81. DOI: 10.1016/s1525-1578(10)60455-2 [PubMed: 12707371]
45. Jain AK. Data clustering: 50 years beyond K-means. Pattern Recognition Letters. 2010; 31(8):651–66.
46. Honarkhah M, Caers J. Stochastic Simulation of Patterns Using Distance-Based Pattern Modeling. Mathematical Geosciences. 2010; 42(5):487–517. DOI: 10.1007/s11004-010-9276-7

47. Brocchieri L. Phylogenetic Diversity and the Evolution of Molecular Sequences. Journal of Phylogenetics & Evolutionary Biology. 2015

48. Wyatt AW, Azad AA, Volik SV, Annala M, Beja K, McConeghy B, et al. Genomic Alterations in Cell-Free DNA and Enzalutamide Resistance in Castration-Resistant Prostate Cancer. JAMA oncology. 2016; doi: 10.1001/jamaoncol.2016.0494

49. Tannock IF, Hickman JA. Limits to Personalized Cancer Medicine. The New England journal of medicine. 2016; 375(13):1289–94. DOI: 10.1056/NEJMsb1607705 [PubMed: 27682039]

50. Scher HI, Lu D, Schreiber NA, Louw J, Graf RP, Vargas HA, et al. Association of AR-V7 on Circulating Tumor Cells as a Treatment-Specific Biomarker With Outcomes and Survival in Castration-Resistant Prostate Cancer. JAMA oncology. 2016; doi: 10.1001/jamaoncol.2016.1828

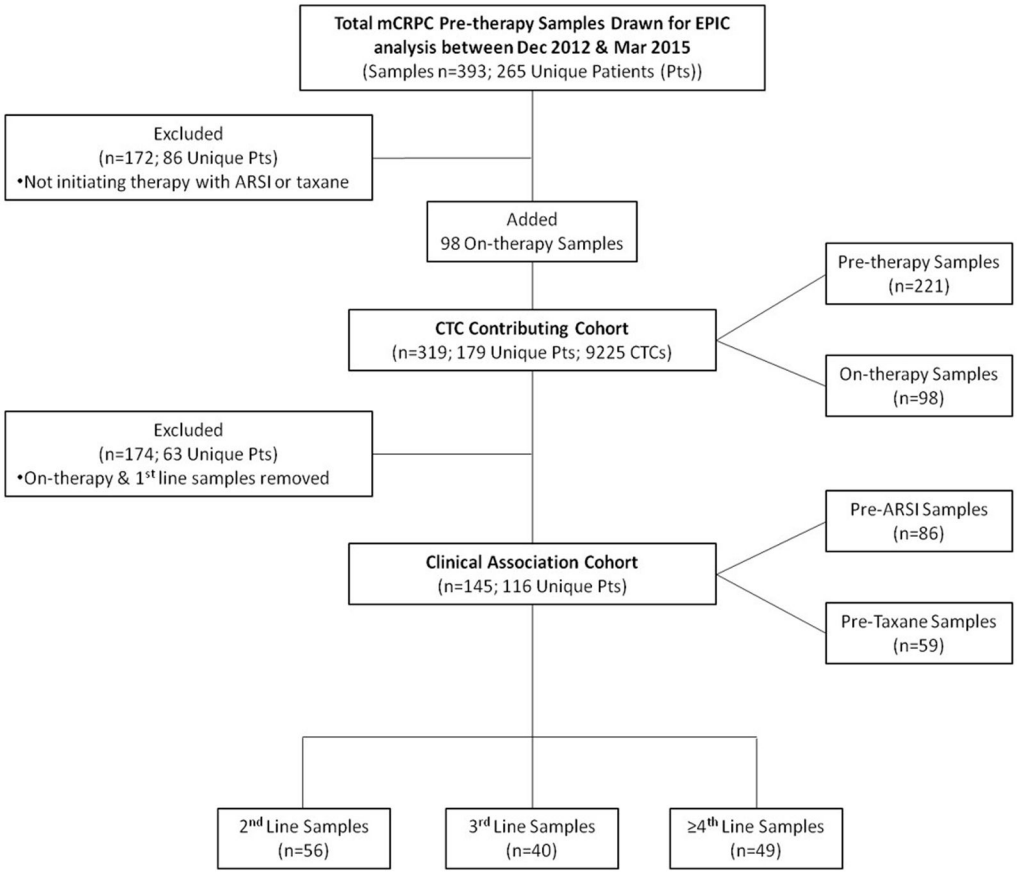

Figure 1. The Distribution of Patient Samples in the CTC Contributing Cohort and Clinical Association Cohort

CONSORT diagram showing the breakdown of patient samples analyzed for this study. Displayed from top to bottom is the total number of samples collected, samples included for CTC digital pathology for unsupervised clustering and phenotypic assessment (CTC Contributing Cohort), and the subset of samples used for the clinical association cohort, by therapy class administered and line of therapy.

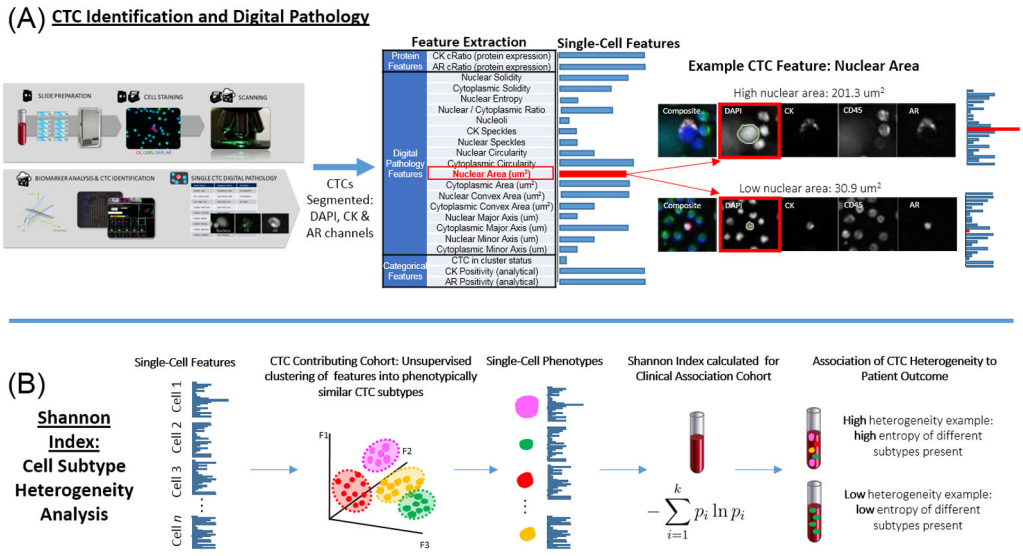

Figure 2. CTC and Clinical Association Analysis Overview

Shown are schematics for **(A)** CTC detection and digital pathology analysis on single cells, as well as generation of patient-level quantification of phenotypic heterogeneity by **(B)** Shannon index.

(A)

Cell Type	Distinguishing Phenotypic Features
A	Low cytokeratin, no AR, huge cell size
B	High CK expression, AR overexpression, large cytoplasm
C	No AR expression, large cytoplasm
D	Very small cell and nuclear size, high CK expression
E	Distinctly high AR expression, high nuclear entropy
F	High CK expression, AR expression, frequently in histological cluster of 2 CTCs
G	Very high CK expression and frequent high AR expression
H	Low AR expression, spindly cell shape
I	Low CK expression, Low AR expression, frequently found in histological CTC clusters
J	Very small cell size, high n/c ratio
K	Huge nucleus, high n/c ratio
L	Very small cell, frequent AR overexpression, high n/c ratio
M	Huge nuclear size, high nuclear entropy
N	Non-circular cell shape
O	Low AR expression, high nuclear entropy, large cell size

(B)

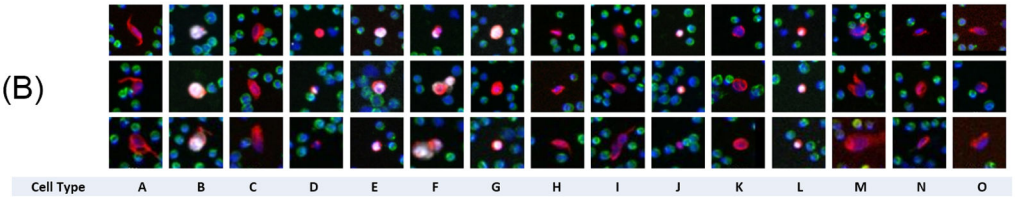

Figure 3. Phenotypic cell types resulting from unsupervised clustering

(A) Shorthand description of each cell type's distinguishing features. **(B)** Example images of each cell type. Blue = DAPI (DNA), Red = cytokeratins, green = CD45, white = AR. Note that AR signal indicates AR protein overexpression.

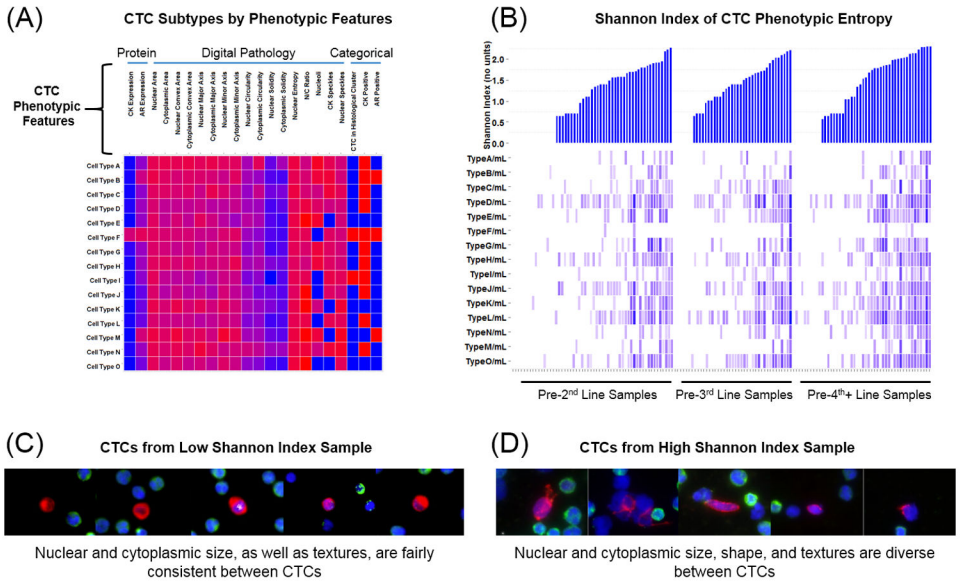

Figure 4. CTC Phenotypic Features, Cell Subtype Classifications, and Shannon Index of CTC Phenotypic Entropy in Patient Samples

(A) CTC phenotypic features included in this analysis and unsupervised clustering of the CTC phenotypic features identified across all CTCs in the CTC Contributing Cohort (n=9225) was used to categorize CTCs into 15 phenotypic subtypes (‘A’-’O’). Shown is a heat map of mean individual cell features per phenotypic subtype. High = red, low = blue. **(B)** Heat map of CTC phenotype densities detected per patient sample, organized by line of therapy. The bar plot above shows the resulting Shannon index by samples from the observed intra-sample diversity of CTC phenotypes. **(C)** An example of CTCs from a low Shannon index sample. **(D)** An example of CTCs from a high Shannon index sample.

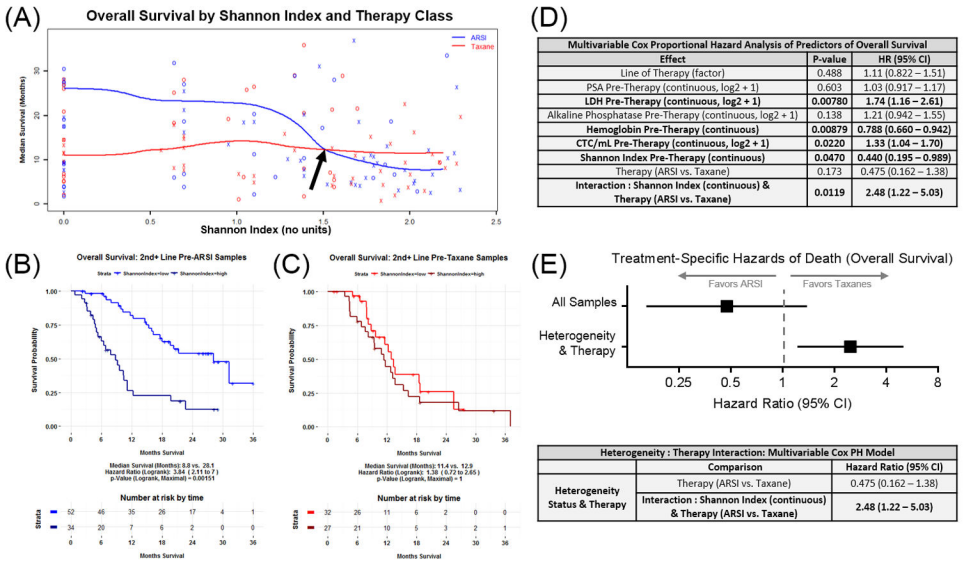

Multivariable Cox Proportional Hazard Analysis of Predictors of Overall Survival		
Effect	**P-value**	**HR (95% CI)**
Line of Therapy (factor)	0.488	1.11 (0.822 – 1.51)
PSA Pre-Therapy (continuous, log2 + 1)	0.603	1.03 (0.917 – 1.17)
LDH Pre-Therapy (continuous, log2 + 1)	**0.00780**	**1.74 (1.16 – 2.61)**
Alkaline Phosphatase Pre-Therapy (continuous, log2 + 1)	0.138	1.21 (0.942 – 1.55)
Hemoglobin Pre-Therapy (continuous)	**0.00879**	**0.788 (0.660 – 0.942)**
CTC/mL Pre-Therapy (continuous, log2 + 1)	**0.0220**	**1.33 (1.04 – 1.70)**
Shannon Index Pre-Therapy (continuous)	**0.0470**	**0.440 (0.195 – 0.989)**
Therapy (ARSI vs. Taxane)	0.173	0.475 (0.162 – 1.38)
Interaction : Shannon Index (continuous) & Therapy (ARSI vs. Taxane)	**0.0119**	**2.48 (1.22 – 5.03)**

Heterogeneity : Therapy Interaction: Multivariable Cox PH Model		
	Comparison	**Hazard Ratio (95% CI)**
Heterogeneity Status & Therapy	Therapy (ARSI vs. Taxane)	0.475 (0.162 – 1.38)
	Interaction : Shannon Index (continuous) & Therapy (ARSI vs. Taxane)	**2.48 (1.22 – 5.03)**

Figure 5. The Degree of Inter-Sample Shannon Index is Related to Overall Survival of ARSI, but not Taxanes

(A) The relationship between degree of heterogeneity (Shannon index, x-axis) and overall survival (y-axis) is shown, along with nonparametric kernel estimates of median survival. Colors represent treatment received after pre-therapy draw. “O” = patient alive at last observation, “X” = patient died at time indicated. Overall Survival is alternately visualized with Kaplan-Meier plots from patients starting **(B)** ARSI and **(C)** Taxanes with survival curves dichotomized with the survival crossover point from **(A)**, indicated with an arrow. Individual covariates were tested for additive power to predict overall survival using a Cox proportional hazards (PH) model. **(D)** The resulting p-values, hazard ratios, and 95% confidence intervals. **(E)** The interaction of therapy and heterogeneity integrated into the multivariate Cox PH model. The forest plot shows hazard ratios and 95% confidence intervals.

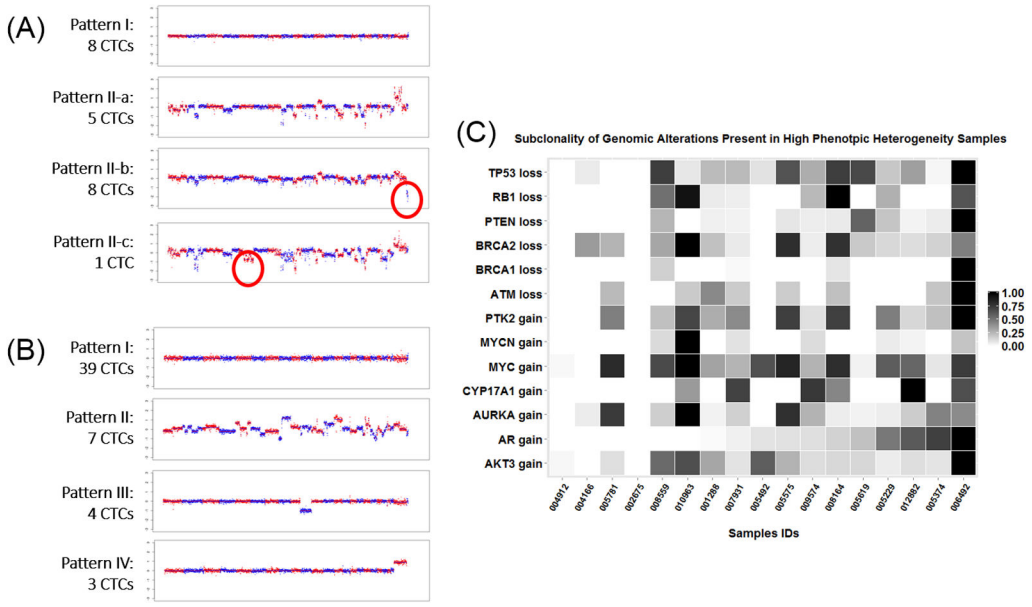

Figure 6. Heterogeneous Genomic Profiles Observed in High Phenotypic Heterogeneity Samples

Copy number variation plots are displayed in parts **A** and **B**, where chromosomes are shown left to right, 1 to 22, X and Y, odd as red, even as blue. Log2 normalized copy number ratio (sample/reference) is indicated on the y-axis for two patient samples that exhibited high CTC phenotypic heterogeneity (by both Shannon index and Pleomorphism index). **(A)** Red circles indicate chromosome Y loss and a chr5q deletion that were observed in sub-patterns of genomic pattern II. All cells identified for this patient are visualized here. **(B)** The four dominant profiles found across 53 of the 62 individual cells sequenced are illustrated. **(C)** Heatmap of degree of subclonality of genomic alterations present in high phenotypic heterogeneity samples, with tile darkness indicating the proportion of single-cell whole genome sequenced CTCs with the indicated genomic alteration per sample. Black tiles indicate complete clonality of a given alteration, and white indicate complete absence. Gray tiles indicate degrees of sub-clonality.

Table 1

Demographics and Sample Characteristics of the CTC Contributing Cohort and Clinical Association Cohort

	CTC Contributing Cohort	Clinical Association Cohort
Patient Characteristics		
Unique Patients	179	116
Age, years: median (range)	68 (45–91)	69 (48–91)
Primary Treatment		
Prostatectomy	84 (47%)	55 (48%)
Radiation	34 (19%)	20 (17%)
Brachytherapy	7 (4%)	7 (6%)
None	54 (30%)	34 (29%)
Sample Characteristics		
Total Baseline (pre-therapy) Samples	221	145
Follow-up (on-therapy) Samples	98	0
Total Samples	319	145
Samples with CTCs	264	131
Prior Hormone Therapies at Baseline [a]		
1–2 lines	82 (37%)	25 (17%)
3 lines	50 (23%)	38 (26%)
4 or more lines	89 (40%)	82 (57%)
Chemotherapy Status at Baseline		
Chemo-naïve	136 (62%)	63 (43%)
Chemo-exposed	85 (38%)	82 (57%)
Metastatic Therapy Initiated after Baseline		
ARS Inhibitor	150	86 (59%)
Taxane	71	59 (41%)
Line of Metastatic Therapy at Baseline		
1st line	76	0
2nd line	56	56
3rd line	40	40
≥4th line	49	49
Metastatic Sites of Disease at Baseline		
Bone Only [b]	66 (30%)	46 (32%)
Lymph Node Only [b]	24 (11%)	10 (7%)

	CTC Contributing Cohort	Clinical Association Cohort
Bone and Lymph Node [b]	93 (42%)	63 (43%)
Bone and Visceral +/− LN [b]	35 (16%)	25 (17%)
Soft Tissue Only	3 (1%)	1 (1%)
Laboratory Measures at Baseline		
PSA, ng/mL: median (range)	37.7 (0.1–3728.2)	62.7 (0.1 – 3728.2)
Hgb, g/dl: median (range)	12 (7–15)	11.6 (7 – 15)
ALK, unit/L: median (range)	110 (25–2170)	121 (42 – 1816)
LDH, unit/L: median (range) [c]	222.5 (123–1293)	238.5 (123 – 1004)
ALB, g/dl: median (range)	4.2 (31.–4.9)	4.2 (3.1 – 4.9)
AR N-term CTC Test at Baseline		
Total CTC/mL: median (range)	6.3 (0–991.3)	6.25 (0–991.3)

[a]- includes GnRH agonists and antagonists, antiandrogens and next-generation hormonal therapies (abiraterone acetate, enzalutamide, and apalutamide)

[b]- includes patients with other soft tissue disease

[c]- three samples did not have LDH available